OECD Workshop on Iodine Aspects of Severe Accident Management
Vantaa, Finland, May 18-20, 1999, NEA/CSNI/R(99)7

A SIMPLIFIED MODEL FOR CONTAINMENT IODINE CHEMISTRY AND TRANSPORT: MODEL DESCRIPTION AND VALIDATION USING STAINLESS STEEL RTF TEST RESULTS

J.C. Wren, G.A. Glowa and J.M. Ball
AECL Chalk River Laboratories, Ontario, Canada K0J 1J0
wrenc@aecl.ca glowag@aecl.ca ballj@aecl.ca

ABSTRACT

A model (IMOD-1.0) for the simulation of containment iodine chemistry and transport has been developed. The model consists of a small set of chemical reactions and transport phenomena which can be described by differential equations. IMOD-1.0 was created in response to a need for a compact model that is easy to understand and use, and can be readily incorporated into containment safety analysis codes. IMOD treats the transport and adsorption of iodine and adsorption of iodine onto surfaces in the same manner as LIRIC (Library of Iodine Reactions in Containment). However, in IMOD-1.0, the numerous rate equations for aqueous phase processes in LIRIC have been reduced to a pair of empirical reactions. Rate constants for these empirical reactions have been extracted from parametric calculations using LIRIC over a wide range of conditions. IMOD-1.0 is based on the full-scale mechanistic database, but has the advantages of a small model. The validation of this model has commenced, using Radioiodine Test Facility (RTF) data from a series of tests performed in stainless steel vessels. This paper describes the model, and presents simulation data compared to experimentally collected RTF data.

1. INTRODUCTION

We have constructed a simple iodine model, IMOD-1.0 (Iodine Module for Containment Codes) that can be used to determine iodine volatility in containment under postulated accident conditions. This simple model, developed from extensive sensitivity analysis of the comprehensive mechanistic LIRIC model (Wren, 1997), consists of two aqueous phase iodine reactions, aqueous iodine and surface interaction, aqueous-gas phase interfacial mass transfer, and iodine sorption on gas phase surfaces. The model has been validated with some of the experimental data obtained with stainless steel vessels in the Radioiodine Test Facility (RTF) (Wren, 1999-1). This report presents the validation of the model IMOD-1.0 using RTF tests, some of which were performed as part of the wok-in-kind under the COG/IPSN PHEBUS FP agreement.

2. DESCRIPTION OF IMOD 1.0

2.1 General Model Description

The simplified containment iodine chemistry and transport model, IMOD-1.0, groups iodine species into six categories: non-volatile and volatile iodine species in the aqueous phase (NONVOLI(aq) and VOLI(aq)), non-aqueous iodine species (NONAQI), iodine species in the gas phase (VOLI(g)), iodine in condensing water film on surfaces (I(con)), and iodine on the surfaces in contact with the gas phase (I(ad)).

The reactions and the transport processes of these species in IMOD-1.0 are schematically presented in Figure 1.

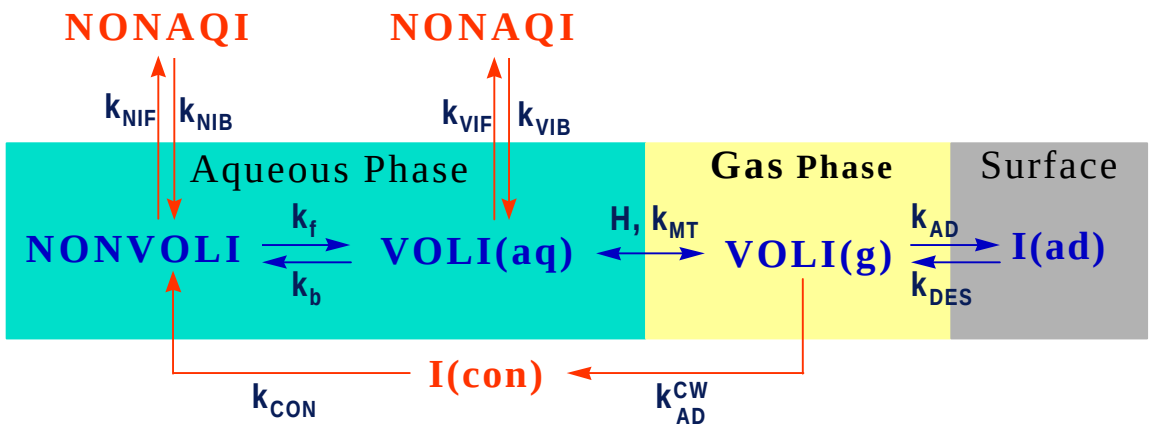

Fig. 1 Iodine Pathways in IMOD-1.0: k represents a pseudo first order rate constant.

Reaction pathways and transport between these six groups of iodine species are formulated using simple first order differential equations. The reactions and mass transport processes considered in the first version of the model are:

(1) two aqueous phase iodine reactions,
(2) aqueous iodine and surface interaction,
(3) aqueous-gas phase interfacial mass transfer of volatile iodine,
(4) iodine sorption on dry surfaces in contact with the gas phase,
(5) iodine sorption on condensing walls, followed by transport of condensate to the bulk water phase.

Each iodine reaction path in IMOD-1.0 represents many steps, so the first order rate constants for these reactions are overall or effective rate constants. They have been defined as a function of radiation dose, temperature, pH, type of surface, surface area, gas and aqueous volume, based on parametric studies of LIRIC.

2.2 Derivation of Rate Constants

The set of differential equations used to describe the processes in Figure 1 are listed in Table 1. The first order rate constants used in these differential equations are defined in Table 2. The rate constants in Table 2 have been derived from parametric calculations using the LIRIC data-base, or from experimental studies. A brief rationalization of some of the choices for these constants follows. A complete description is provided in the literature (Wren,1999-1).

Table 1 Differential Equations In IMOD-1.0*

#	Equation
A	$\frac{d[NONVOLI(aq)]}{dt}=-k_f\cdot[NONVOLI(aq)]+k_b\cdot[VOLI(aq)]-k_{NIF}\cdot[NONVOLI(aq)]+k_{NIB}\cdot[NONAQI]$
B	$\frac{d[VOLI(aq)]}{dt}=k_f\cdot[NONVOLI(aq)]-k_b\cdot[VOLI(aq)]-k_{VIF}\cdot[VOLI(aq)]+k_{VIB}\cdot[NONAQI]$
C	$\frac{d[NONAQI]}{dt}=k_{NIF}[NONVOLI(aq)]+k_{VIF}[VOLI(aq)]-k_{NIB}[NONAQI]-k_{VIB}[NONAQI]$
D	$\frac{d([VOLI(g)])}{dt}=k_{MT}\cdot\frac{A_{int}}{V_g}\cdot([VOLI(aq)]-([VOLI(g)]\cdot H_{VOLI}))$
F	$\frac{d([VOLI(aq)])}{dt}=k_{MT}\cdot\frac{A_{int}}{V_{Aq}}\cdot(([VOLI(g)]\cdot H_{VOLI})-[VOLI(aq)])$
G	$\frac{d([VOLI(g)])}{dt}=-k_{AD}\cdot[VOLI(g)]\cdot\left(1-\frac{[I(ad)]}{SAT}\right)$
H	$\frac{d([I(ad)])}{dt}=k_{AD}\cdot\frac{V_g}{A_g}\cdot[VOLI(g)]\cdot\left(1-\frac{[I(ad)]}{SAT}\right)$
I	$\frac{d([VOLI(g)])}{dt}=k_{DES}\cdot\frac{A_g}{V_g}\cdot[I(ad)]$
J	$\frac{d([I(ad)])}{dt}=-k_{DES}\cdot[I(ad)]$
K	$\frac{d([I(con)])}{dt}=k_{AD}^{cw}\cdot[VOLI(g)]\cdot\frac{V_g}{V_{con}}$
L	$\frac{d([VOLI(g)])}{dt}=-k_{AD}^{cw}\cdot[VOLI(g)]$
M	$\frac{d([I(con)])}{dt}=-k_{con}\cdot[I(con)]$
O	$\frac{d([NONVOLI(aq)])}{dt}=k_{con}\cdot[I(con)]\cdot\frac{V_{con}}{V_{aq}}$

* Note that the differential equations are grouped according to the type of processes. For example, the change in [NONVOLI(aq)] due to the aqueous phase reactions is formulated in Equation (A) and the change due to condensation in Equation (O). To obtain the overall change of [NONVOLI(aq)] the terms on the right-hand sides of Equations (A) and (O) should be added.

Aqueous Phase Reactions

Rate constants for inter-conversion of volatile and non-volatile iodine species (k_f and k_b in Equations (A) and (B) in Table 1) were taken directly from analysis of LIRIC calculations performed at various conditions of pH, temperature and dose-rate. These calculations established that Reaction (1) below is the rate determining step for oxidation of iodide to molecular iodine (conversion of non-volatile iodide to volatile iodine) over a large range of conditions. The overall rate constant for conversion of NONVOLI(aq) to VOLI(aq), in IMOD 1.0 (k_f), was therefore defined as the product of the rate constant for Reaction 1, with the concentration of •OH radical (Equation (2)).

$$I^- + \bullet OH \rightarrow I\bullet + OH^- \quad (1)$$

The change in the NONVOLI(aq) concentration due to this reaction can be formulated as

$$\frac{d[NONVOLI(aq)]}{dt} \approx k_1 \cdot [\bullet OH] \cdot [NONVOLI(aq)] = k_f \cdot [NONVOLI(aq)] \quad (2)$$

The rate constant k_1 is 1.1×10^{10} $dm^3 \cdot mol^{-1} \cdot s^{-1}$ (Wren, 1999-1). The concentration of •OH, as determined by LIRIC (Wren, 1999) has a linear dependence upon dose-rate ($[\bullet OH]_{ss}$ ($mol \cdot dm^{-3}$) ≈ $0.90 \times 10^{-12} \times D_r$), hence k_f (s^{-1}) = $(0.010 \pm 0.001) \times D_r$, where D_r is the absorbed dose rate in units of $kGy \cdot h^{-1}$.

Sensitivity studies using LIRIC have also shown that for a given radiation field, pH, dissolved oxygen concentration and temperature, VOLI(aq) and NONVOLI(aq) will tend toward and remain in a near steady-state (Equation 3).

$$K_{aqI} = \frac{[VOLI(aq)]}{[NONVOLI(aq)]} = \frac{k_f}{k_b} \quad . \quad (3)$$

From parametric calculations of the steady-state concentration of VOLI(aq) using the full LIRIC model and values of k_f defined as in Equation (2), the backward rate constant (k_b) used in IMOD-1.0, was calculated as a function of pH, temperature and dose rate (Table 2).

For the simulations of the tests in the presence of silver, the formation of AgI is accounted for in the aqueous phase reaction as

$$VOLI(aq) \rightarrow NONAQI \text{ (i.e. AgI)} \quad (4)$$

where: k_{VIF} (s^{-1}) $= \nu_{Ag} \cdot (A_{Ag}/V_{aq})$
ν_{Ag} (dms^{-1}) is the deposition velocity of I_2 on Ag
A_{ag} (dm^2) is the geometric surface area of the silver metal
V_{aq} (dm^3) is the volume of the aqueous phase

The iodine interaction with Ag is considered to be irreversible, therefore the reverse of Reaction (4) was set to 0 (i.e. $k_{VIB} = 0$). The same deposition velocity ν_{Ag} was used for the simulation of PHEBUS RTF 3, which contained two "adsorption stages", and PHEBUS RTF 6 (see Section 3). These experiments contained 30 g and 200 g of Ag in the aqueous phase, respectively.

Mass Transfer

The interfacial mass transfer coefficient k_{MT} for high mixing and non-condensing conditions was obtained from a specifically commissioned RTF experiment performed under flow conditions typical of many RTF experiments (Evans, 1990). The temperature dependence of the individual (k_{maq} and k_{mg}) gas and liquid phase mass transfer coefficients was based on the known temperature dependence of the diffusion coefficients for species in the gas and aqueous phase. The PHEBUS RTF experiments were performed under less vigorous mixing conditions in the gas phase, with some tests performed under non-condensing and the others under condensing conditions. For the

non-condensing PHEBUS RTF tests, a gas phase mass transfer rate constant an order of magnitude lower than that for high mixing conditions was used. For the condensing PHEBUS RTF tests, the gas phase mass transfer rate constant was the same as that for the high mixing and non-condensing conditions, but an aqueous phase mass transfer rate constant an order of magnitude higher was used. These increases in the mass transfer coefficients are considered to be reasonable because an increase in the convection flow will result from condensation. It should be noted that a same mass transfer rate constant is used for a given set of conditions. (See Table 2).

Table 2 Rate Constants And Parameters

Constant	Rate
k_f (s^{-1})	$(0.01 \pm 0.001)\cdot D_r$ (D_r in units of $kGy\cdot h^{-1}$)
k_b (s^{-1})	$k_b = A_b\cdot\exp(-\Delta E_b/RT)\cdot[H^+]^{-n}\cdot(D_r)^{½}$ $n = (0.80 \pm 0.04) + (500 \pm 25)\cdot(1/T - 1/298)$ $A_b = (8 \pm 2) \times 10^{16}$ $\Delta E_b = (134 \pm 2) \times 10^3$ $J\cdot mol^{-1}$ ($[H^+]$ in units of $mol\cdot dm^{-3}$, T in units of Kelvin, and R is 8.314 $J\cdot mol^{-1}\cdot K^{-1}$)
k_{NIF} (s^{-1})	default = 0
k_{NIB} (s^{-1})	default = 0
k_{VIF} (s^{-1})	default = 0, $k_{VIF} = \nu_{Ag}\cdot(A_{Ag}/V_{aq})$ in the presence of aqueous phase silver, where $\nu_{Ag} = (0.010 \pm 0.005)$ $dm\cdot s^{-1}$ [a], and A_{Ag} is the silver surface area in dm^2 (A_{Ag}/V_{aq} has units of dm^{-1})
k_{VIB} (s^{-1})	default = 0
k_{mg} [b] ($dm\cdot s^{-1}$)	1×10^{-1} (T/298) for mixing and non-condensing conditions 1×10^{-2} (T/298) for non (or little)-mixing and non-condensing 1×10^{-1} (T/298) for condensing conditions
k_{maq} [b] ($dm\cdot s^{-1}$)	7×10^{-4} $(T/298)^{2/3}$ for mixing and non-condensing conditions 7×10^{-3} $(T/298)^{2/3}$ for condensing conditions
H_{VOLI}	$\ln(H_{VOLI}) = \ln(H_{I2(298K)}) + (-\Delta G_{VOLI}/R) \times (1/298 - 1/T)$ $H_{I2(298K)} = (79 \pm 8)$ $\Delta G_{VOLI}/R = (3600 \pm 200)$ or $\Delta G_{VOLI} = (30 \pm 2)$ $kJ\cdot mol^{-1}$
k_{AD} (s^{-1})	$= \nu_{AD}\cdot(A_g/V_g) = 1 \times 10^{-2}\cdot(A_g/V_g)$
k_{DES} (s^{-1})	$\ln\left(k_{DES}\right) = \ln(k_{DES(298K)}) + \left(\frac{\Delta E_{DES}}{R}\right)\cdot\left(\frac{1}{298} - \frac{1}{T}\right)$ $k_{DES(298K)} = (9 \pm 2) \times 10^{-7}$ s^{-1} $\Delta E_{DES} = (74.6 \pm 1.5)$ $kJ\cdot mol^{-1}$
k_{AD}^{CW} (s^{-1})	$k_{AD}^{CW} = \nu_{AD}^{CW}\cdot(A_{con}/V_g)$ $\nu_{AD}^{CW} = (7 \pm 2) \times 10^{-4}$ $dm\cdot s^{-1}$
SAT($mol\cdot dm^{-2}$)	default = 2×10^{-6}
k_{con} (s^{-1})	$= F_{con}/V_{con}$

Note: T, pH, V_g, V_{aq}, V_{con}, A_{int}, A_g, F_{con} are defined by boundary conditions

[a] ν_{Ag} was calculated assuming that A_{ag} was the geometric surface area of the silver. This simple assumption results in a deposition velocity which is artificially high, and faster than mass transfer should allow. However, this effect is negated when surface area is used again for the calculation of the first order rate constant (i.e., $\nu_{Ag}\cdot(A_{Ag}/V_{aq})$)

[b] Used in the calculation of k_{MT}: $\frac{1}{k_{MT}} = \frac{1}{k_{maq}} + \frac{H_{VOLI}}{k_{mg}}$

The partition coefficient, (H), for VOLI in IMOD-1.0 is defined to be that of I_2 (Wren, 1999-1). H is a thermodynamic equilibrium constant, therefore it is assumed to follow a simple

Arrhenius temperature dependence as shown in Table 2. Because of this simplifying assumption which bases the overall partition coefficient for iodine only on I_2, IMOD 1.0 predicts iodine volatility less accurately if organic iodide formation in the aqueous phase is significant, which is likely to be the case with organic-painted vessels. Nonetheless, because of the wide ranges of types of organic iodides and their corresponding partition coefficients (Wren, 1999-2), the average partition coefficient of organic iodides that would be formed may be not that far off that for I_2.

Adsorption/Desorption

Among the reaction parameters in IMOD-1.0, the adsorption and desorption parameters are the most difficult to define. This is not because of the difficulty in formulating the iodine sorption process for a given surface, but because of the difficulty in defining the surface characteristics and surface area properly. This problem is less serious for smooth structures, such as painted carbon steel, whose surface area can be well defined using the geometric surface area and on which the iodine is deposited rather uniformly. For metal surfaces, however, iodine deposition may be initiated and localized on defect sites. Furthermore, the surface characteristics may change with adsorption, as a result of corrosion. The iodine adsorption/desorption on dry surfaces is included in IMOD-1.0 as a first order process (see Equations 6 and 7 in Table 2), with the adsorption rate constant k_{AD} further defined as:

$$k_{AD} = \nu_{AD} \cdot (A_g/V_g) \tag{5}$$

where ν_{AD} ($dm \cdot s^{-1}$) is the adsorption rate constant per unit area per volume, referred to as the surface deposition velocity, A_g(dm^2) is the area of the surface exposed to the gas phase, and V_g(dm^3) is the volume of the gas phase.

For the simulations of the tests performed under non-condensing conditions, the iodine adsorption/desorption rate constants for electropolished and untreated stainless steel were chosen on the basis of experimental studies performed on the deposition of molecular iodine on stainless steel coupons (Wren, 1999-3). Where applicable, adsorption onto painted coupons in the gas phase was included in the calculations. This value was also chosen on the basis of experimental studies (Wren, 1997). Iodine desorption from painted coupons was not included because it is thought that adsorption on to epoxy painted surfaces is an irreversible chemisorption process.

The rate constant for absorption of iodine in condensing water films in IMOD-1.0 (k_{AD}^{CW}) was extracted from simulations of the PHEBUS RTF 5 test (see Section 3). The transport of the condensing film from the wall to the bulk water, which maintains a steady state volume of the condensing film on the wall is included as a first order process. The rate of the first order transport of the condensing film (k_{con}) was experimentally determined from the volume flow rate of the film, F_{con}, divided by the volume of the film V_{con}. Iodine desorption from condensed water on walls was not included because iodine is quickly hydrolyzed to I^- upon contact with the condensing film.

3. VALIDATION OF THE MODEL

Predictions of the containment iodine model IMOD-1.0 have been compared against the results of various RTF tests performed in stainless steel vessels. The model simulation results for six RTF tests are described in this report. Three of these experiments were designed to examine the effect of a series of pH adjustments on iodine volatility from irradiated solutions of CsI at temperatures of 25 and 90°C. An additional three tests at 90°C examine the effects of condensing conditions, and/or the presence of Ag metal in the aqueous phase on irradiated aqueous solutions of CsI. Experiments performed at higher temperature also contained painted epoxy coupons in the gas phase and the aqueous phase.

Simulations of the RTF test results are described below. The experiments were simulated by solving the kinetics of the reaction schemes listed in Table 1 with the rate constants listed in Table 2. This was accomplished using FACSIMILE[1], a commercially available numerical integration package for simultaneously solving coupled differential equations.

3.1 Description of the RTF Tests

The RTF itself, and typical RTF test procedure and test conditions are described in detail elsewhere (Ball, 1997). A summary of the conditions of the experiments used for this modelling exercise is presented in Table 3.

Table 3 RTF Test Conditions

Condition	P0T2	Phebus RTF2A	Phebus RTF2B	Phebus RTF3	Phebus RTF5	Phebus RTF6
Vessel electropolished	316L no	316L yes	316L yes	316L yes	316L yes	316L yes
Dose Rate ($kGy \cdot h^{-1}$)	~ 1.36	~ 0.9	~ 0.9	~ 0.8	~ 0.7	~ 0.8
Sump Temperature	25 °C	90 °C	90 °C	90 °C	90 °C	90 °C
Wall Temperature	25°C	110 °C	110 °C	110 °C	80 °C	80 °C
Initial [CsI] ($mol \cdot dm^{-3}$)	9×10^{-6}	1×10^{-5}	1×10^{-5}	1×10^{-5}	1×10^{-5}	1×10^{-5}
Aqueous Volume (dm^3)	25	30	30	30	30	30
Gas Volume (dm^3)	315	310	310	310	310	310
Starting pH	10	9	4.5	4.5	4.5	9
Surface Area[a]: gas(dm^2) aqueous(dm^2)	220 52	220 52	220 52	220 52	220 52	220 52
Coupons[b]: (gas) (aqueous)	no no	3@250 cm^3 8@19cm^2	3@250 cm^3 8@19cm^2	3@250 cm^3 8@19cm^2	3@250 cm^3 8@19cm^2	3@250 cm^3 8@19cm^2
Ag (grams)	no	no	no	32	no	200
Boric acid ($mol \bullet dm^{-3}$)	no	no	0.3	0.3	0.3	0.3

[a] vessel surface areas only (loop area excluded)
[b] Hydrocentrofugon 901 Ripolin White- epoxy paint

[1] FACSIMILE - AEA Technologies, Harwell Laboratory, Oxfordshire, UK.

For the experiments performed in the absence of silver metal, the test observations can be summarized as follows:

(1) the gas phase iodine concentration, [I(g)], increased with a decrease in pH,
(2) for a given pH and temperature the gas phase iodine concentration, [I(g)], initially increased with time, and later followed a slow exponential (almost linear) decrease,
(3) the total aqueous phase iodine concentration, [I(aq)] and, where applicable the condensate iodine concentration, [I(con)] slowly decreased exponentially with time, and
(4) the gas phase iodine concentration was slightly larger under condensing conditions (PHEBUS RTF 5) than under non-condensing conditions (PHEBUS RTF 2).

The presence of Ag in the aqueous phase resulted in an exponential decrease in [I(aq)], [I(g)], and [I(con)] which was much greater than that observed in the absence of Ag. The rate constant for this exponential decay decreased with an increase in pH.

3.2 Simulations and Discussion

3.2.1 RTF P0T2

The simulation results of P0T2 Stage 1 and 2 with IMOD-1.0, are shown in Figures 2 to 5. The calculated results are in good agreement with the observed gas and aqueous phase concentrations over a wide range of pH conditions at 25°C (within a factor of three for the gas phase concentration).

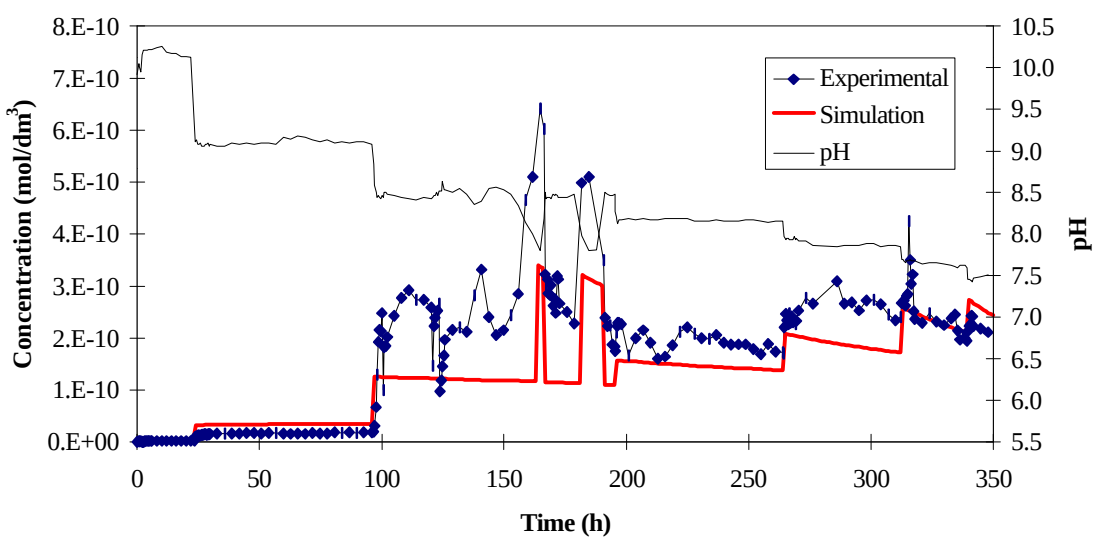

Fig. 2 Calculated vs. experimental results for the total amount of iodine (mol·dm^{-3}) in the gas phase, P0T2 Stage 1.

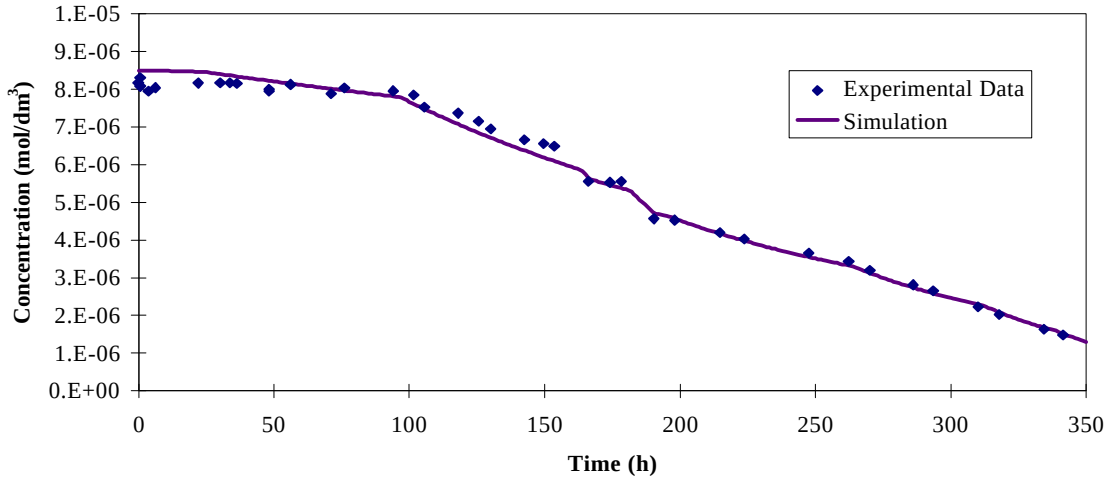

Fig. 3 Calculated vs. experimental results for the total amount of iodine (mol·dm^{-3}) in the aqueous phase P0T2 Stage 1.

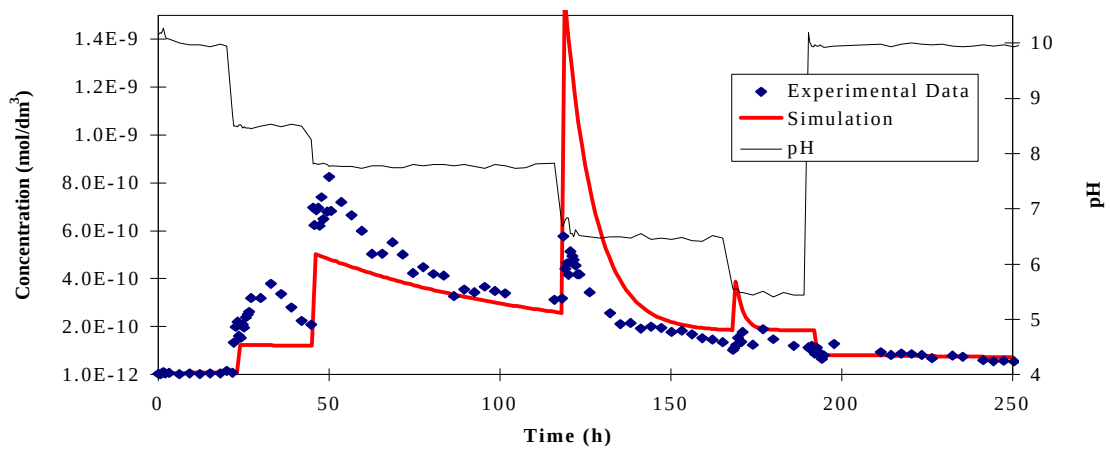

Fig. 4 Calculated vs. experimental results for the total amount of iodine (mol·dm^{-3}) in the gas phase, P0T2 Stage 2.

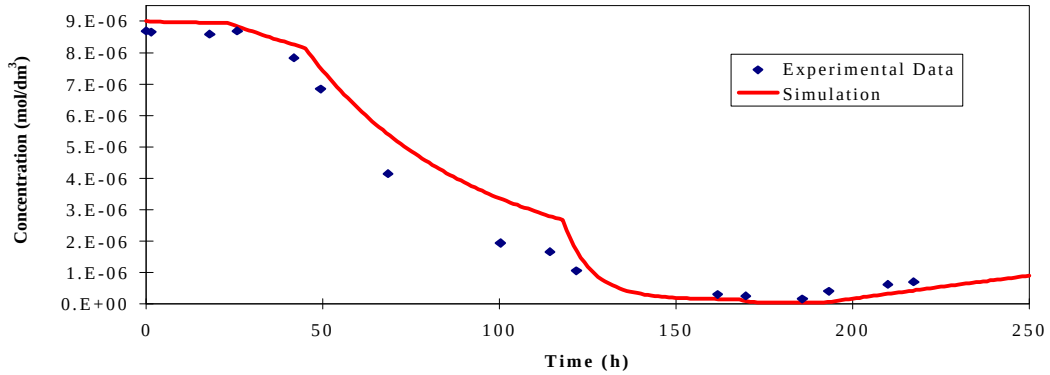

Fig. 5 Calculated vs. experimental results for the total amount of iodine (mol·dm^{-3}) in the aqueous phase P0T2 Stage 2.

3.2.2 PHEBUS RTF 2A and 2B

These tests were performed at 90°C, under non-condensing conditions and in the absence of silver. The simulation results for the gas and aqueous phase iodine concentrations are shown relative to the experimental data in Figures 6 through 9.

The gas phase iodine concentrations at the beginning of Test 2B increased much more slowly than expected (Figure 8). The cause of this slow increase is not due to the accumulation of iodine in the gas phase being limited by the rate of interfacial mass because this slow change was not observed during sudden pH changes (cf. Figure 4). Adsorption of iodine on surfaces in the aqueous phase is also ruled out as a possible cause, because the adsorption of iodine on the surface would have drastically reduced the aqueous iodine concentration. The shape of the initial curve of the gas phase iodine concentration in Test 2B indicates that reactions such as;

$$\text{VOLI(aq)} + \text{Impurity(aq)} \leftrightarrow \text{Iodine Complex(aq)} \quad (6)$$

$$\text{Impurity(aq)} \rightarrow \text{Decomposition Products} \quad (7)$$

may be occurring in the aqueous phase. For example, I_2 may react with organic impurities to establish a fast equilibrium with a non-volatile charge transfer complex, which could subsequently undergo radiolytic decomposition to release VOLI(aq), (and VOLI(g)). Alternatively, I_2 may be reacting with active sites on the stainless steel surfaces in contact with the aqueous phase to form FeI_2, which is readily dissolved in the aqueous phase to release I^-. Assuming a finite number of active iron sites, this process would produce the same observed effect as the organic impurity scheme. At this point we do not have experimental data to confirm either of the explanations.

The proposed mechanism was tested in the simulation of the PHEBUS RTF test 2B[2]. The simulation result suggests that a reaction such as proposed above may be required to explain the observed gas phase iodine behaviour at the beginning of the test.

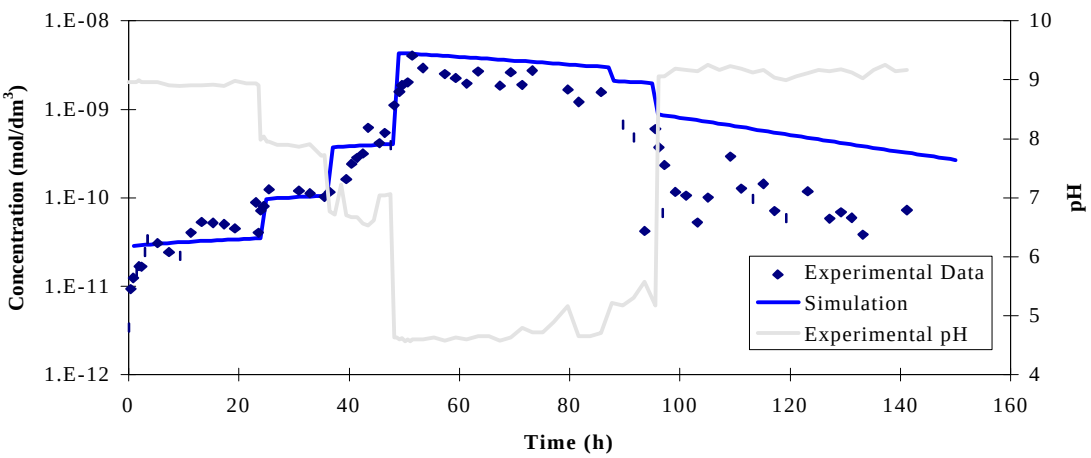

Fig. 6 Calculated vs. experimental results for the total amount of iodine ($mol \cdot dm^{-3}$) in the gas phase, PHEBUS RTF 2A

[2] One of the calculations shown in Figure 8 was obtained using 1×10^3 $dm^3 \cdot mol^{-1} \cdot s^{-1}$ and 2.5×10^{-3} s^{-1} for the forward and backward rate constant of Equilibrium (6) and 8×10^{-5} s^{-1} for the decomposition rate of Reaction (7) and 1×10^{-3} $mol \cdot dm^{-3}$ for the impurity level.

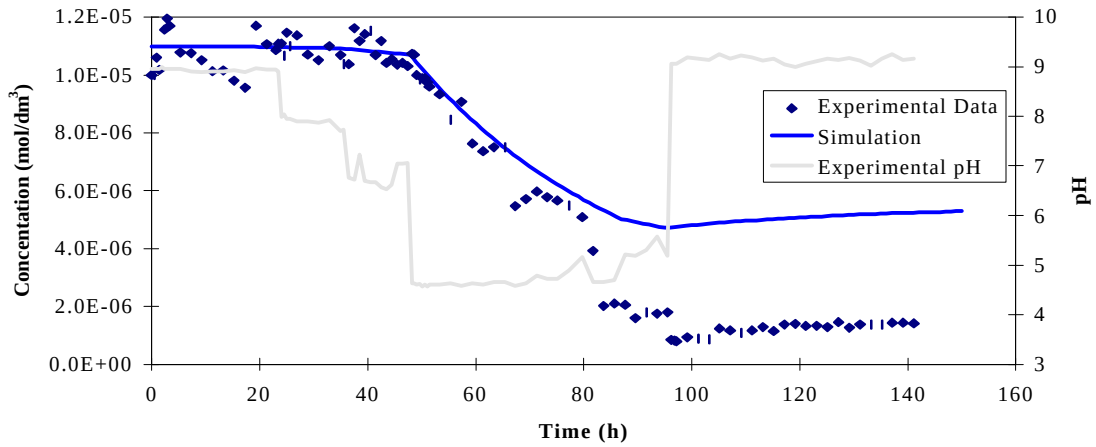

Fig. 7 Calculated vs. experimental results for the total amount of iodine (mol•dm^{-3}) in the aqueous phase, PHEBUS RTF 2A

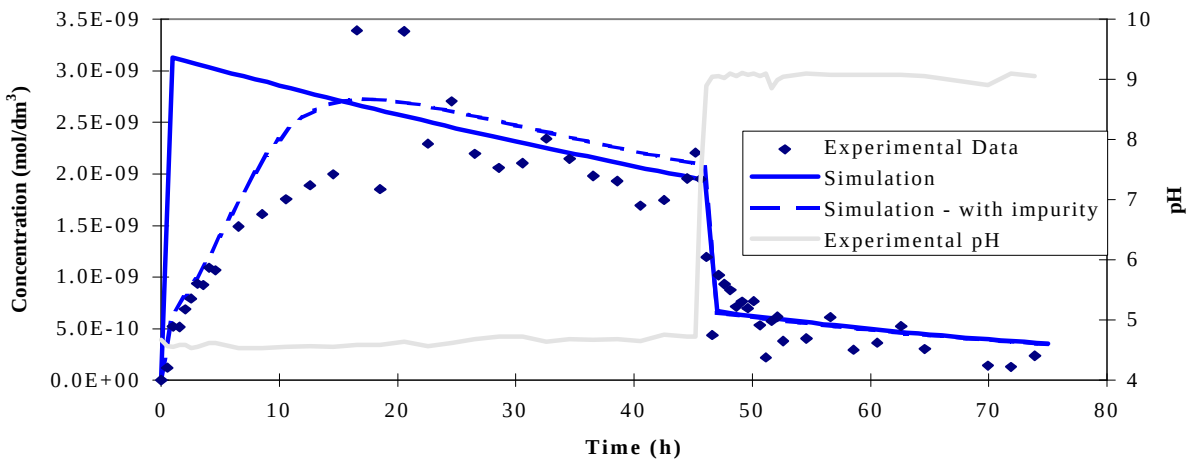

Fig. 8 Calculated vs. experimental results for total amount of iodine (mol•dm^{-3}) in the gas phase, PHEBUS RTF 2B

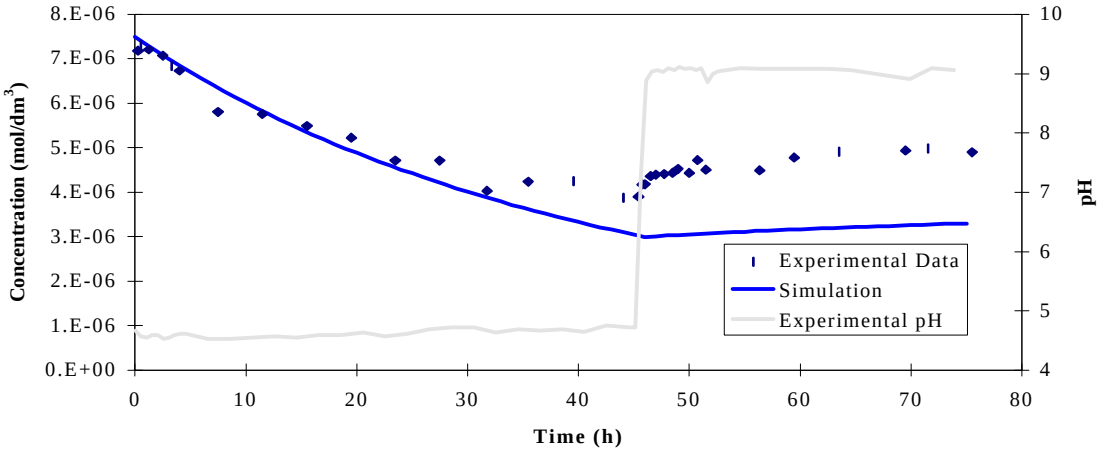

Fig. 9 Calculated vs. experimental results for the total amount of iodine (mol•dm^{-3}) in the aqueous phase, PHEBUS RTF 2B

3.2.3 PHEBUS RTF 5

The simulation results of PHEBUS RTF Test 5 performed under condensing conditions, are shown in Figures 10 and 11. The exponential decrease in the aqueous phase iodine concentration in PHEBUS RTF 5 is slower than that observed in the similar experiment RTF 2B. This is because the decrease in RTF 5 is due only to iodine adsorption on the painted coupons. In RTF 5, any iodine that adsorbs onto the condensed water film returns to the aqueous phase and therefore there is no net loss of iodine to the vessel walls.

As was observed in simulations of RTF2B, the calculated concentration of iodine in the gas phase and the condensate at the beginning of the test are higher than those observed. Similar reaction mechanisms (Reaction (6) and (7)) suggested for PHEBUS RTF 2B are also considered to be responsible for this case.

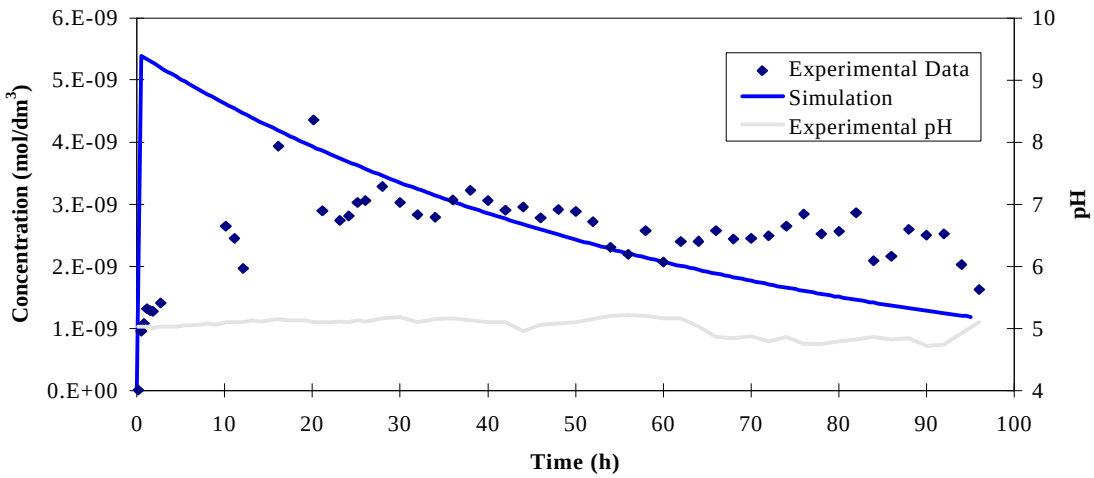

Fig. 10 Calculated vs. experimental results for the total amount of iodine (mol·dm^{-3}) in the gas phase, PHEBUS RTF 2B

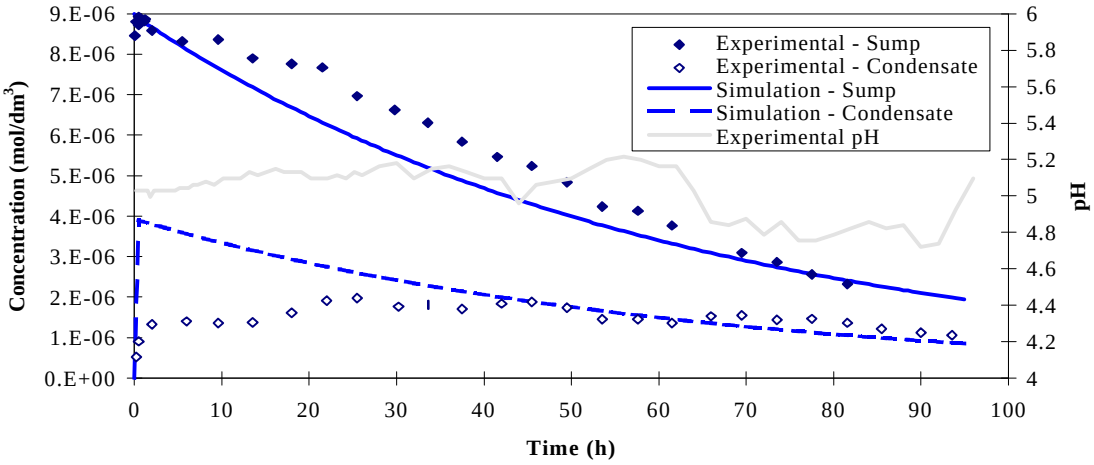

Fig. 11 Calculated vs. experimental results for the total amount of iodine (mol·dm^{-3}) in the aqueous phase, PHEBUS RTF 2B

3.2.4 PHEBUS RTF 3 and PHEBUS RTF 6

The results of PHEBUS RTF Tests 3 and 6 are shown in Figures 12 to 15. With silver metal in the aqueous phase, the iodine reaction with silver dominated the behaviour of iodine in the aqueous phase.

In PHEBUS RTF 6, there was a significant delay between starting the test, and the onset of the exponential decrease of iodine in the aqueous phase. An explanation for this observation is that in both Tests 3 and 6, the silver wool was housed in a container made of stainless steel mesh. Because of the larger mass of silver used in RTF 6, as compared to RTF 3, there was more contact of Ag with stainless steel in the former. When AgI is in contact with iron, the following reaction is known to occur (Greenwood, 1985):

$$AgI + Fe \rightarrow Ag + FeI_2 \quad (8)$$

FeI_2 dissolves easily in water, to release I^-. The release of I^- from AgI was confirmed in separate controlled experiments in which AgI was placed in contact with Fe powder, stainless steel filings and stainless steel coupons. The overall impact of this reaction would be to delay the deposition of iodine on silver. The proposed mechanism was tested in the simulation of PHEBUS RTF 6 shown in Figures 14 and 15. The simulation included Reaction (8) until 25 h, after which reactive Fe is assumed to be exhausted. The mechanism appears to account for the iodine behaviour.

An important feature about the modelling of the Ag/iodine interactions in this experiment is that a simple mechanism, using direct interaction of silver metal with I_2 in the aqueous phase, and the same deposition velocity for both stages of RTF3 and for RTF6, adequately reproduced the results of both RTF3 and RTF6. This simple mechanism appears to explain the pH dependence of the reaction, and the observed decrease of aqueous phase iodine concentration very well, and it was not necessary to invoke the formation of AgO, or the reaction between silver metal and iodide ion.

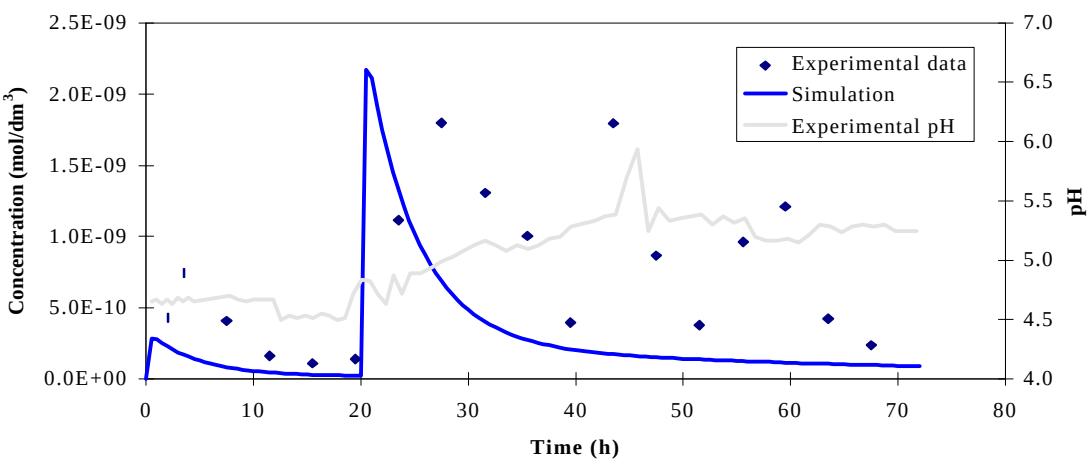

Fig. 12 Calculated vs. experimental results for the total amount of iodine ($mol \cdot dm^{-3}$) in the gas phase, PHEBUS RTF 3. Note that the increase in aqueous phase iodine at 21 h was due to an intentional second addition of CsI.

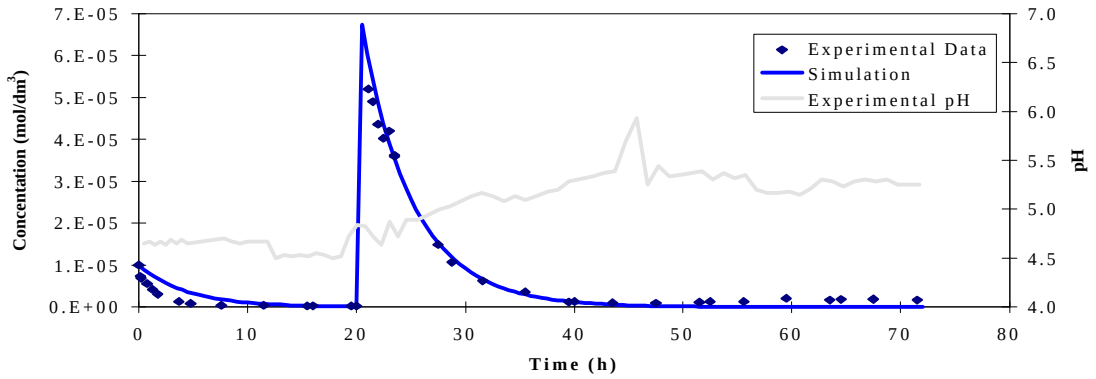

Fig. 13 Calculated vs. experimental results for the total amount of iodine (mol·dm^{-3}) in the aqueous phase, PHEBUS RTF 3. Note that the increase in aqueous phase iodine at 21 h was due to an intentional second addition of CsI.

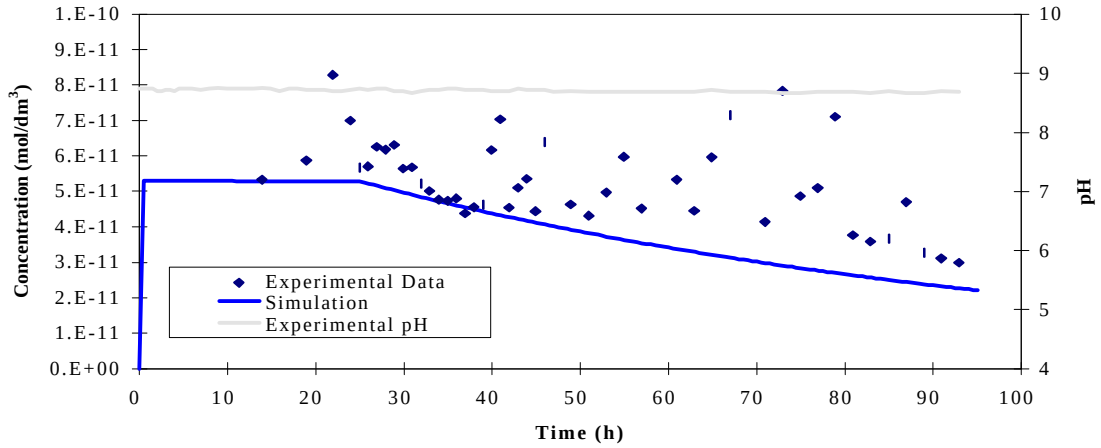

Fig. 14 Calculated vs. experimental results for the total amount of iodine (mol·dm^{-3}) in the gas phase, PHEBUS RTF 6.

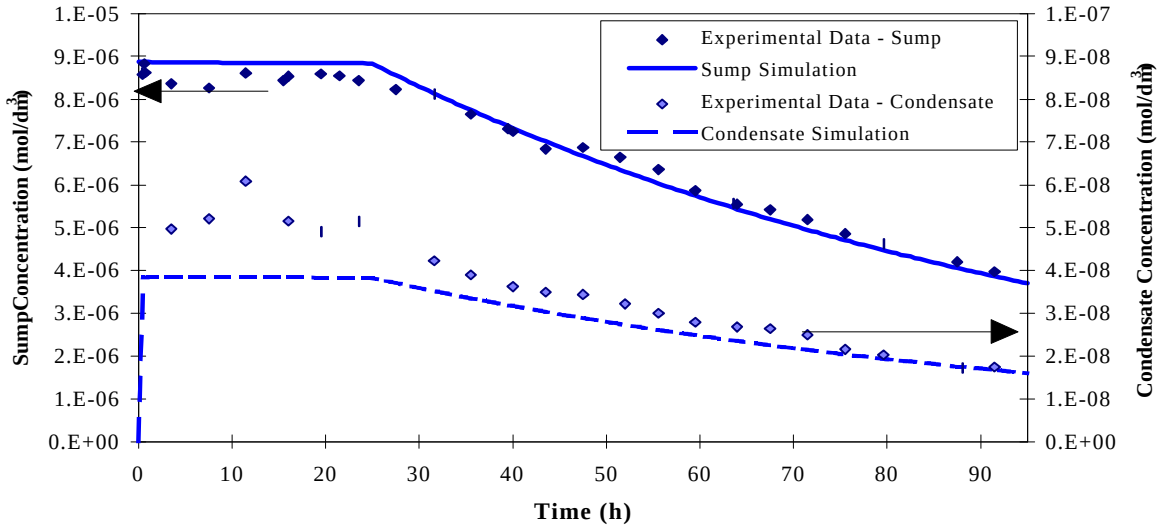

Fig. 15 Calculated vs. experimental results for total amount of iodine (mol·dm^{-3}) in the aqueous phase, PHEBUS RTF 6.

4. CONCLUSIONS

Simulation calculations of PHEBUS RTF tests using the simple iodine model, IMOD-1.0, have been performed as part of the validation of the model. The model can reproduce experimental results obtained under controlled pH conditions ranging from pH 4 to 9, and at temperatures of 25 and 90°C and iodide concentrations between 10^{-6} and 10^{-4} mol•dm^{-3} Condensing conditions and rapid aqueous adsorption onto silver are also successfully simulated using this simple model. The gas phase iodine concentration is reproduced within a factor of two, except during the early transient periods. The model reproduced the iodine concentrations in the aqueous phase and in the condensate to within 20%. The model requires further development in some areas, particularly in organic iodide formation and pH prediction, and the effective rate constants will be refined to expand the applicability of the model to wider ranges of conditions and to minimize the uncertainties in the model predictions.

ACKNOWLEDGMENTS

The work reported in this document was partially funded by the COG R&D Program: Working Party 06, Containment Behaviour, WPIR No. 425, and 600 under the joint participation of Ontario Hydro, Hydro Quebec, New Brunswick Power and AECL.

REFERENCES

Ball, J.M. et. al. 1999. International Standard Problem (ISP) no. 41**.** in Proceedings of OECD Workshop on Iodine Aspects of Severe Accident Management, Vantaa, Finland, May 18-20.

Ball, J.M., Kupferschmidt, W.C.H. and Wren, J.C., 1997. Phase 2 Radioiodine Test Facility Experimental Program, In Proceedings of the Fourth CSNI/OECD Workshop on the Chemistry of Iodine in Reactor Safety, Wurenlingen, Switzerland, 1996, p. 63.

Evans, G.J., Melnyk, A., Paquette, J., and Sagert, N. H. 1990. The LIRIC Database/Model, in Proceedings of 2nd International Conference on Containment Design and Operation, Toronto Canada, Canadian Nuclear Society.

Wren, J.C., Glowa, G.A., and Ball J.M., 1997. Modelling Iodine Behaviour using LIRIC 3.0, in Proceedings of the Fourth CSNI/OECD Workshop on the Chemistry of Iodine in Reactor Safety, Wurenlingen, Switzerland, 1996, p. 507.

Wren, J.C., Glowa, G.A. and Ball, J.M., 1999-1 A Simplified Model for Containment Iodine Chemistry and Transport Part I: Model Description and Validation Using Stainless Steel RTF Test Results. *to be published*.

Wren, J.C., Ball J.M., and Glowa, G.A., 1999-2. The Interaction of Iodine with Organic Material in Containment. *Nuclear Technology* **125**, 337-362.

Wren, J.C., Glowa, G. A., Merrit, J., 1999-3. Corrosion of Stainless Steel by Gaseous I_2. *Journal of Nuclear Materials*, **265**, 161-177.

Greenwood, N.N., and Earnshaw, A., 1985. *The Chemistry of the Elements*, Pergamon, New York, p. 933.